Article

Site and Structural Requirements for the Dehydra-Decyclization of Cyclic Ethers on ZrO$_2$

Mengjie Fan [1], Yichen Ji [1], Ajibola Lawal [2], Omar A. Abdelrahman [2], Raymond J. Gorte [1] and John M. Vohs [1,*]

[1] Department of Chemical and Biomolecular Engineering, University of Pennsylvania, Philadelphia, PA 19104, USA

[2] Department of Chemical Engineering, University of Massachusetts Amherst, 686 N. Pleasant Street, Amherst, MA 01003, USA

[*] Correspondence: vohs@seas.upenn.edu; Tel.: +1-215-898-6318

Abstract: In this study, we examined the site and structural requirements for the dehydra-decyclization of cyclic ethers, tetrahydrofuran, and tetrahydropyran to produce conjugated dienes over ZrO$_2$-based catalysts, a reaction that could be an important step in the use of biomass-derived sugars as a starting material to produce monomers for the plastics industry. To help identify the active sites for this reaction, studies were conducted in which ZrO$_2$ surfaces were decorated with Na. These studies showed that Na was effective at poisoning the activity for the ring opening of cyclic ethers, but much less so for the dehydration of the resulting adsorbed alkoxides. The studies of the activity of different types of ZrO$_2$ for the dehydra-decyclization reaction, including single crystals and ultra-thin films supported on MgAl$_2$O$_4$ and silica, also showed that the reaction was dependent on the local structure of the ZrO$_2$ surface. The insights these results provide for identifying the active sites on the ZrO$_2$ surface are discussed.

Keywords: zirconia oxide; dehydra-decyclization; cyclic ether; diene; biomass

1. Introduction

Recently, there has been much interest in the use of C$_6$ and C$_5$ sugar molecules produced by hydrolysis of cellulose, as a renewable feedstock for the production of fuels and chemicals [1–3]. The initial steps in many of the proposed pathways for upgrading these biomass-derived sugars to more useful products are dehydration followed by hydrogenation to produce furanic molecules [4–6]. Aldol condensation reactions with these furanic molecules can be used to increase the carbon number if the goal is to produce hydrocarbons for use as fuels or lubricants [6–9]. It has also been shown that dehydra-decyclization of these cyclic ethers can be used to produce conjugated dienes [10–12]. This pathway is particularly interesting since the dienes have high value for use as monomers for production of synthetic rubber (e.g., acrylonitrile-butadiene-styrene (ABS) and adiponitrile) [13,14].

It has been demonstrated in several studies that dehydra-decyclization of cyclic ethers to dienes (see Scheme 1) can be achieved with relatively high selectivity using solid Brønsted acids [10,12,15]. For example, H-ZSM-5 and amorphous SiO$_2$/Al$_2$O$_3$ are active for this reaction and capable of achieving reasonably high yields [15,16]; however, strong Brønsted acids promote the oligomerization of the product dienes, which in turn leads to catalyst deactivation and loss in selectivity [17,18]. Although the much weaker acid, H-[B]ZSM-5, was shown to be capable of converting 2-methyltetrahydrofuran (2-MTHF) to pentadienes with a yield of 89% and better stability, rates on this material are low [19]. To address this issue, Ji et al. explored the use of metal oxides, such as ZrO$_2$, to catalyze the dehydra-decyclization reaction [20]. They observed that tetragonal ZrO$_2$ was active and selective for the dehydra-decyclization of C$_4$ and C$_5$ cyclic ethers, obtaining yields greater than 80% for the corresponding conjugated diene products at 673 K. Monoclinic ZrO$_2$ was found to have similar activity to the tetragonal phase but deactivated more rapidly. Although they

speculated that Lewis-acid sites (or exposed Zr^{4+} cations) were likely to be important, the specific active sites for the reaction were not identified.

Scheme 1. (**a**) Dehydra-decyclization of tetrahydrofuran (THF) to 1,3-butadiene. (**b**) Dehydra-decyclization of tetrahydropyran (THP) to 1,3-pentadiene.

In the work reported here, we have explored how the structure of the ZrO_2 affects its activity for the dehydra-decyclization of the cyclic ethers, tetrahydrofuran (C_4H_8O, THF) and tetrahydropyran ($C_5H_{10}O$, THP). Since the ring opening of these cyclic ethers produces adsorbed alkoxides, we also studied the reaction of isopropanol and 4-penten-1-ol (4P1OL) on ZrO_2. Insight into the site requirements for these reactions were obtained by comparing the catalytic properties of bulk ZrO_2 powders with yttria-stabilized, cubic ZrO_2 single crystals (YSZ) and ZrO_2-thin films grown by atomic layer deposition (ALD) on high surface area $MgAl_2O_4$ (MAO) and SiO_2 supports. The effect of poisoning adsorption sites was also used to provide insight into site requirements for the reaction.

2. Results

Previous studies have shown that tetragonal ZrO_2 is active and selective for the dehydra-decyclization of C_4 an C_5 cyclic ethers to produce conjugated dienes at temperatures between 573 and 673 K [20]. Although it was suggested that the reaction proceeds on Lewis-acid sites on the ZrO_2 surface, the specific sites for this reaction have yet to be fully identified. To investigate the role of exposed surface O^{2-} anions and Zr^{4+} cations, we first measured the effect of Na poisoning on the activity of a series of bulk ZrO_2 catalysts.

Figure 1a shows the overall conversions for the reactions of THF at 673 K and isopropanol at 598 K as a function of the weight loading of the Na dopant. More detailed reactivity data are provided in Table 1. Different temperatures were chosen for the two reactions so that the conversions over the pure zirconia were ~50% for each system. For THF, greater than 80% selectivity to butadiene was obtained for all Na coverages; for isopropanol, the only hydrocarbon product was propene. Although selectivity for the THF reaction remained high, the conversion decreased linearly with increasing Na coverage, and the 2 wt% Na sample was inactive for this reaction. This may be due to the adsorbed Na blocking Lewis acid sites, as has been suggested previously [21,22]. Note, however, that adsorbed Na had a lesser effect on the dehydration of isopropanol. For this reaction the conversion also decreased with increasing Na coverage, but the 2 wt% Na sample still exhibited significant activity with a conversion that was ~50% of that on the un-poisoned sample.

Figure 1b shows a similar data set for the reactions of the C_5 cyclic ether, THP, and the unsaturated alcohol, 4-penten-1-ol (4P1OL), on the Na-poisoned ZrO_2 samples. More detailed reactivity data are provided in Table 2. The 4P1OL was used for this comparison because it has been proposed as an intermediate in the dehydra-decyclization of THP over ZrO_2 [23]. For the conditions used here, the primary reaction product for both THP and 4P1OL was 1,3-pentadiene. The trends in these data are similar to those obtained for THF and isopropanol, with the addition of 2 wt% Na completely poisoning the reactivity toward THP but having limited effect on the activity for the dehydration of 4P1OL. More extensive data for the reaction of 4P1OL on ZrO_2 as a function of Na coverage are presented in Figure 2. At 673 K on the Na-free catalyst, the primary reaction product is the desired 1,3-pentadiene (79%). Small amounts of 3-penten-1-ol (5%), 1,4-pentadiene (5%) and butene

(1%) were also produced. Additionally, some cyclization of the 4P1OL reactant occurred to produce 2-methyltetrahydrofuran (9%). This product is significant because it is the reverse of the ring opening reaction and would be expected to occur on the same sites. In addition to causing a decrease in the overall conversion, poisoning the surface with 0.5 wt% Na suppressed the cyclization reaction pathway while maintaining the high selectivity to the desired diene products. These trends continued when the Na level was increased to 2 wt% and for this sample the cyclization reaction did not occur. Together these data indicate that separate sites must be involved in the ring opening of the cyclic ethers and the dehydration of the resulting adsorbed alkoxides.
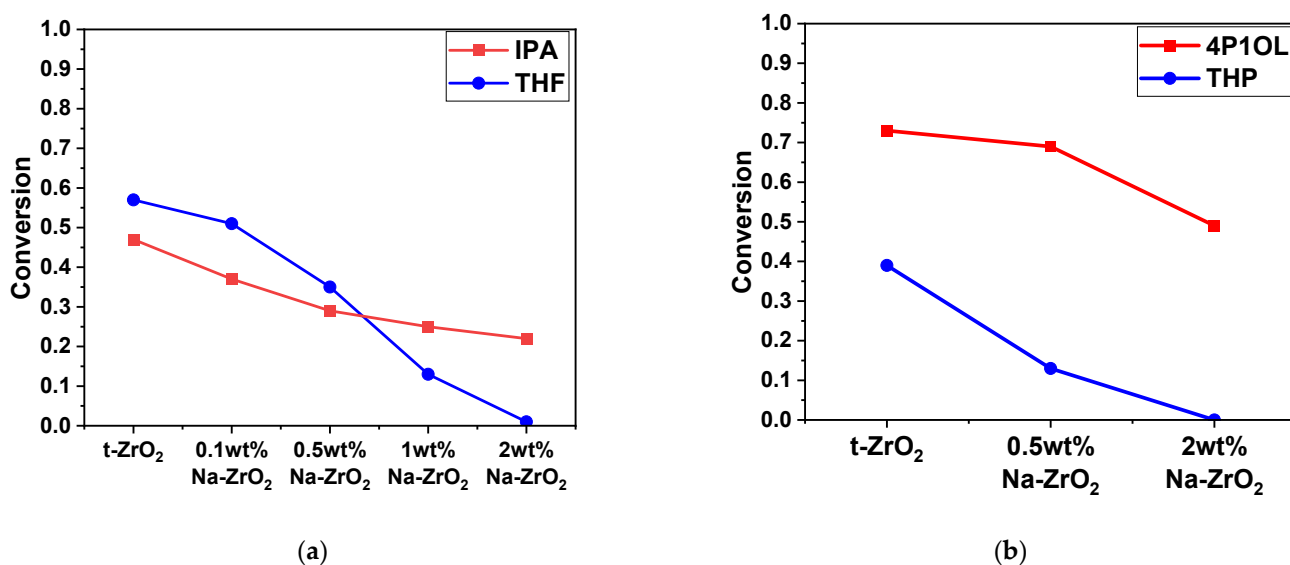

(**a**)

(**b**)

Figure 1. (**a**) Conversion as a function of Na loading for the reaction of isopropanol (IPA) (WHSV = 1.55 g IPA/g cat/h, 598 K) and THF (WHSV = 1.86 g THF/g cat/h, 673 K) on ZrO_2 as a function of the Na loading. (**b**) Analogous data for the reaction of 4P1OL (WHSV = 2.22 g 4P1OL/g cat/h, 673 K) and THP (WHSV = 2.22 g THP/g cat/h, 673 K). Note that blank reaction experiments in which no catalyst was present showed no conversion for both the cyclic ether and alcohol reactants.

Table 1. Conversion and selectivity for reaction of THF (WHSV = 1.86 g THF/g cat/h, 673 K) and IPA (WHSV = 1.55 g IPA/g cat/h, 598 K).

	t-ZrO_2	0.1 wt% Na-ZrO_2	0.5 wt% Na-ZrO_2	1 wt% Na-ZrO_2	2 wt% Na-ZrO_2
THF conversion	0.57	0.51	0.35	0.13	0.01
1,3-butadiene Selectivity *	0.92	0.92	0.92	0.91	0.82
IPA conversion	0.47	0.37	0.29	0.25	0.22
Propene selectivity	1	1	1	1	1

* Other products include CO_2, propene, and butene(s).

Table 2. Conversion and selectivity for reaction of THP (WHSV = 2.22 g THP/g cat/h, 673 K) and 4P1OL (WHSV = 2.22 g 4P1OL/g cat/h, 673 K).

	t-ZrO_2	0.5 wt% Na-ZrO_2	2 wt% Na-ZrO_2
THP conversion	0.39	0.13	0
1,3-pentadiene Selectivity *	0.88	0.89	-
4P1OL conversion	0.91	0.69	0.49
1,3-pentadiene selectivity	0.79	0.72	0.80
2-MTHF Selectivity ‡	0.09	0.03	0

* Other products include butene(s), pentene, 1,4-pentadiene. ‡ Other products include 1,4-pentadiene, pentanol, 3-penten-1-ol, butene(s).
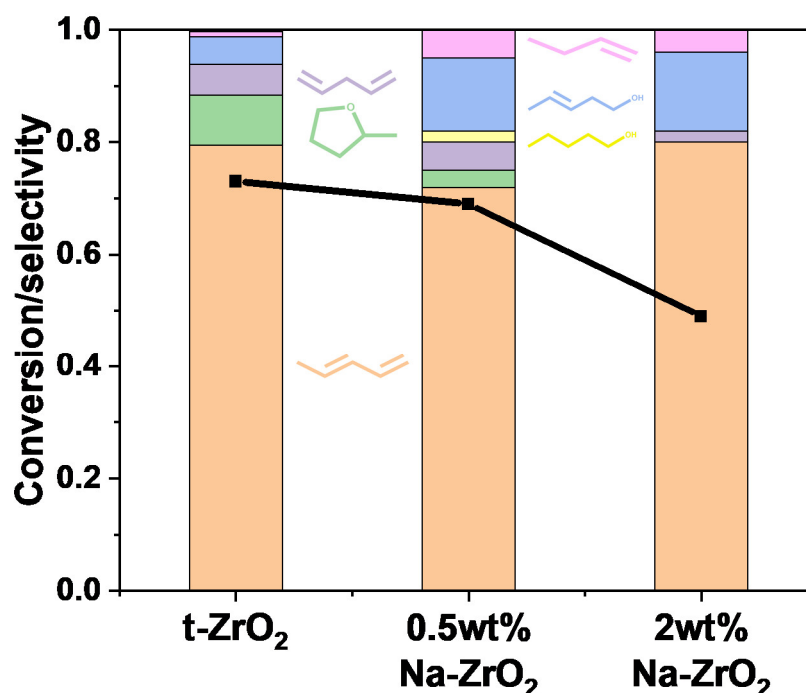
Figure 2. Product distribution for reaction of 4P1OL on ZrO_2 at 673 K as a function of the Na loading (WHSV = 2.22 g 4P1OL/g cat/h). Conversion: ■; color code for product selectivity bars: orange-1,3-pentadiene, green-2-MTHF, purple-1,4-pentadiene, yellow-pentanol, blue-3-penten-1-ol, pink-butene(s).

TPD was also used to study the Na poisoning of reaction sites on the ZrO_2 surface. Figure 3 shows TPD results obtained after room temperature exposure of THF to ZrO_2 pre-covered with 0, 1, or 2 wt% Na. For the un-poisoned ZrO_2, the majority of the adsorbed THF (m/e 72) reacted to produce 1,3-butadiene (m/e 54) at 610 K. A small amount of propene (m/e 41) was also detected at 630 K (not shown). For 1 wt% $Na-ZrO_2$, roughly 70% of the adsorbed THF desorbed intact in a broad peak centered at 420 K and the amount of 1,3-butadiene produced decreased by 50% relative to the Na-free ZrO_2 sample. The 2 wt% $Na-ZrO_2$ was inactive for the reaction of THF to 1,3-butadiene and all the THF reactant desorbed intact from this sample in a peak centered at 400 K.
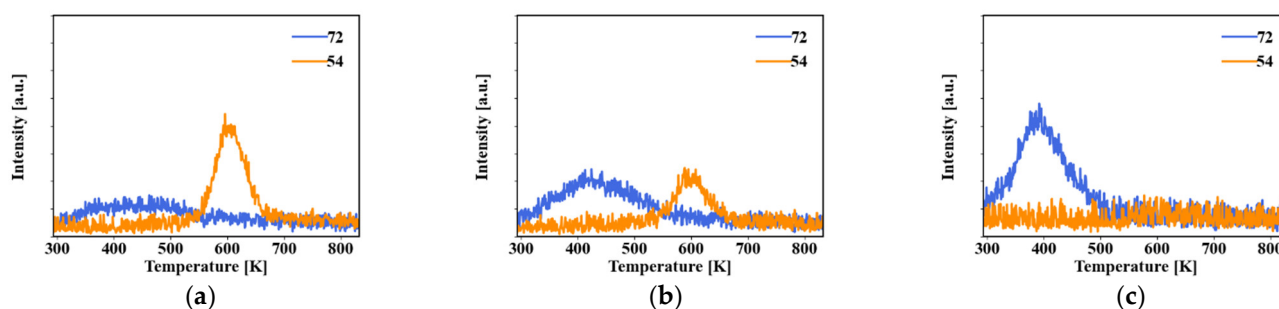

Figure 3. TPD data for the reaction of THF on (**a**) ZrO_2 (**b**) 1 wt% $Na-ZrO_2$ (**c**) 2 wt% $Na-ZrO_2$: THF-m/e 72; 1,3-butadiene-m/e 54.

Analogous TPD results for the reaction of isopropanol on the ZrO_2 samples are presented in Figure 4. Na-free ZrO_2 was active for the dehydration of isopropanol to produce propene (m/e 41), which desorbed in a large peak at 570 K, with a small amount of acetone (m/e 43) also produced at this temperature. Consistent with steady state reaction measurements, increasing the Na coverage resulted in a decrease in reactivity, as indicated by a decrease in the area of the propene (m/e 41) peak. This decrease in peak area, however,

was much less than the corresponding decrease in the THF TPD data, and for the 2 wt% Na-ZrO$_2$ sample, a prominent propene peak was still evident at 600 K.
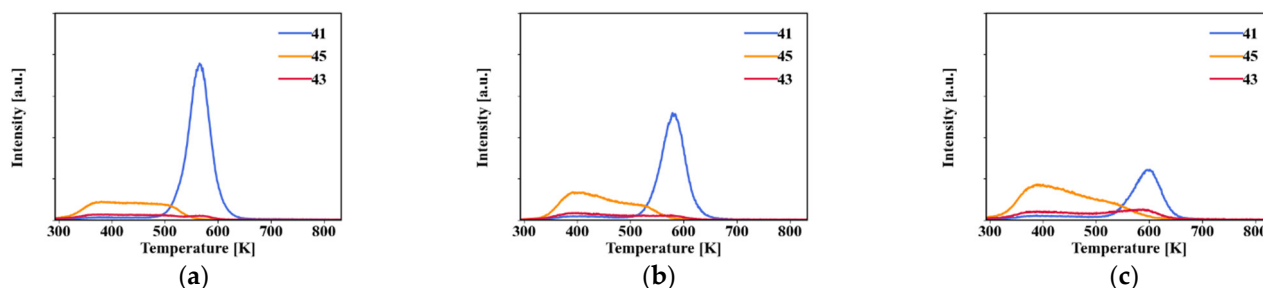

Figure 4. TPD data for the reaction of isopropanol on (**a**) Na-free ZrO$_2$ (**b**) 1 wt% Na-ZrO$_2$ (**c**) 2 wt% Na-ZrO$_2$: isopropanol-m/e 45; propene-m/e 41 at high temperature; acetone-m/e 43 at high temperature.

Both the steady-state reactivity and TPD data for the cyclic ethers and alcohols show that adsorbed Na is highly effective at poisoning the sites involved in the ring opening of THF and THP but has a lesser effect on the dehydration of the adsorbed alcohols (or alkoxides) that are likely intermediates in the dehydra-decyclization reactions. These results again suggest that there may be different types of sites or site pairs on the ZrO$_2$ surface on which ring opening of cyclic ethers and dehydration of alcohols proceed. To further investigate this possibility, we studied the reaction of both alcohols and cyclic ethers on several different types of zirconia, including single-crystal surfaces and ZrO$_2$-thin films that were grown by ALD on both MAO and silica supports.

In the single crystal studies, we used TPD to characterize the reaction of THF on the (100) and (110) planes of the yttria-stabilized, cubic ZrO$_2$ (YSZ). These samples were doped with yttria to stabilize the cubic phase, thereby avoiding the phase transitions, which occur upon heating ZrO$_2$ [24]. Prior studies have shown that YSZ and ZrO$_2$ surfaces have similar activity for the dehydration of alcohols to produce alkenes [25–27]. For example, adsorbed ethanol reacts on YSZ (100) to produce ethylene at 500 K during TPD. Figure 5 displays TPD data obtained in UHV for THF-dosed YSZ (100) and YSZ (110). In contrast to what was observed for alcohols, THF (m/e 72) adsorbed only weakly on both surfaces and desorbed intact below 450 K. No other products, including 1,3-butadiene (m/e 54), were detected during TPD. This result, along with the alcohol TPD studies, shows that the local structure of the ZrO$_2$ surface significantly affects its overall reactivity and that sites active for the ring opening of cyclic ethers, such as THF, are not present on all ZrO$_2$ surfaces.
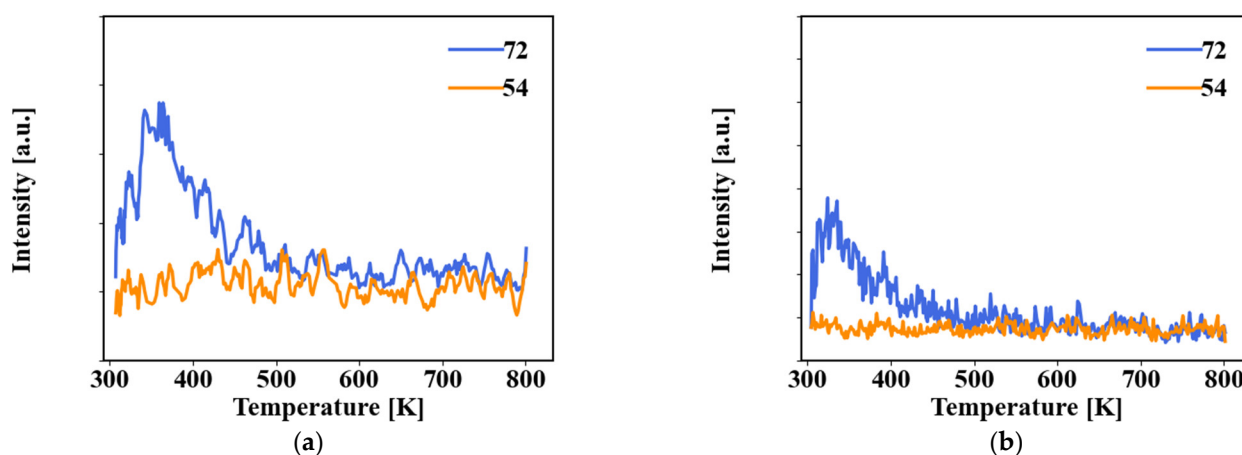

Figure 5. TPD of THF on (**a**) Y-ZrO$_2$(100) and (**b**) Y-ZrO$_2$(110): THF-m/e = 72; 1,3-butadiene-m/e = 54.

As noted above, we also characterized the reactivity of a series of ALD-grown ZrO_2 films, supported on MAO, with nominal thicknesses of 0.2 nm (7 wt%), 0.5 nm (18 wt%), and 1 nm (36 wt%). Isopropanol TPD experiments showed that both the MAO support and the ZrO_2 films were active for the dehydration of isopropanol to produce propene. Figure 6 shows the propene TPD peak (m/e 41) obtained after saturating each sample with isopropanol at 300 K. On the bare MAO support, the reaction occurred at 520 K. After the deposition of ZrO_2, a new propene peak emerged at 590 K, which is consistent with the TPD data for bulk ZrO_2 powder in Figure 4. Using the relative intensities of the peaks at 520 K and 590 K to provide an estimate of the fraction of the surface covered by the ZrO_2 film, these data indicate that the ALD ZrO_2 films are largely conformal to the ALD support, with the 0.5 nm film covering most of the MAO surface and the 1 nm film completely covering the MAO surface.
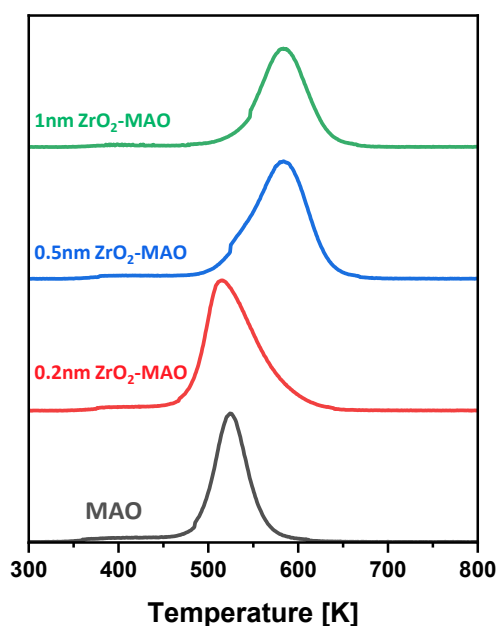

Figure 6. Propene TPD peak (m/e 41) from isopropanol-dosed samples as a function of the ZrO_2 film thickness.

TPD data for the reaction of THF on these thin film samples are shown in Figure 7. For the bare MAO support, THF primarily desorbed intact in a broad peak between 350 and 550 K. The 1,3-Butadiene was not detected as a product from MAO, but a small amount of the adsorbed THF did react to produce propene between 550 and 650 K on this surface (see Figure S3). In contrast, on the ZrO_2 films, THF reacted to produce butadiene at 650 K, consistent with the TPD results for the ZrO_2 powder in Figure 3. The fraction of the adsorbed THF that reacted to produce butadiene on the 0.2 and 0.5 nm ZrO_2 samples was roughly 25%, while, on the 1 nm ZrO_2 film, 40% of the adsorbed THF reacted at 650 K to produce butadiene. The low activity of the 0.2 nm sample may be due to the ZrO_2 film not completely covering the MAO surface; however, this cannot account for the difference in the reactivity of the 0.5 nm and 1 nm films, which both covered the majority of the support.

Conversion and selectivity for the steady-state reaction of THF at 673 K over ZrO_2/MAO thin film catalysts are displayed in Figure 8. The bare MAO support had low activity for ring opening, achieving a conversion of only 23% for these conditions. MAO was also not selective for the desired dehydra-decyclization to butadiene (16%), but rather produced propene (64%) as the primary product. Covering the MAO with a nominal 0.2 nm-thick ZrO_2 film produced an even less reactive catalyst, with a THF conversion of only 5%, although the selectivity for the desired butadiene increased to 62% of the product, with the balance being a mixture of propene and butene. Increasing the ZrO_2 thickness to 0.5 nm increased the THF conversion to only 9%; but the selectivity to butadiene increased to 86%.

The 1 nm ZrO$_2$-MAO sample retained the high selectivity to butadiene (80%) but was much more active with a THF conversion of 64%. These results are consistent with the trends observed in the THF TPD data.
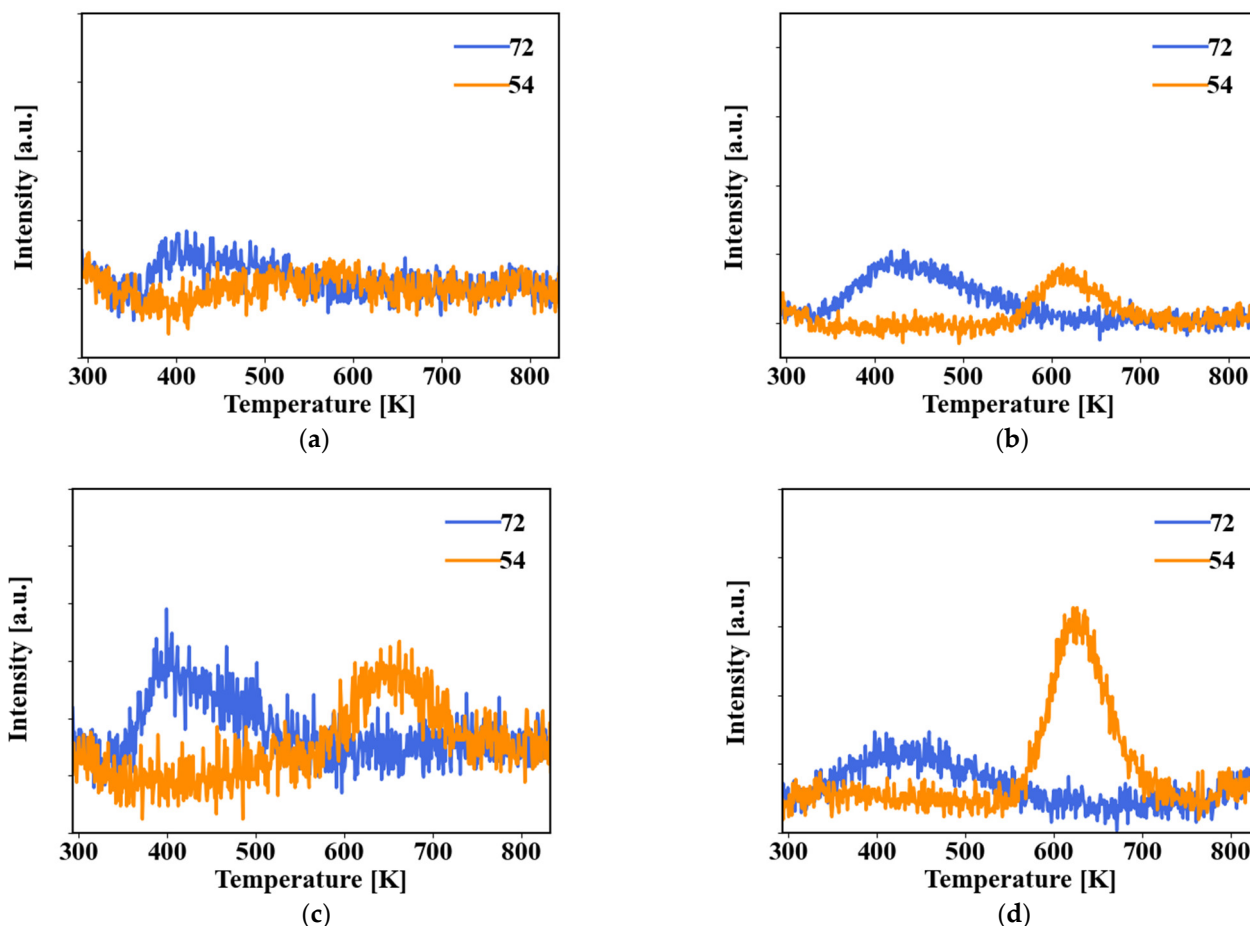

Figure 7. TPD data for THF-dosed (**a**) MAO; (**b**) 0.2 nm ZrO$_2$-MAO; (**c**) 0.5 nm ZrO$_2$-MAO; (**d**) 1 nm ZrO$_2$-MAO. The m/e = 72 and 54 signals correspond to THF and 1,3-butadiene, respectively.
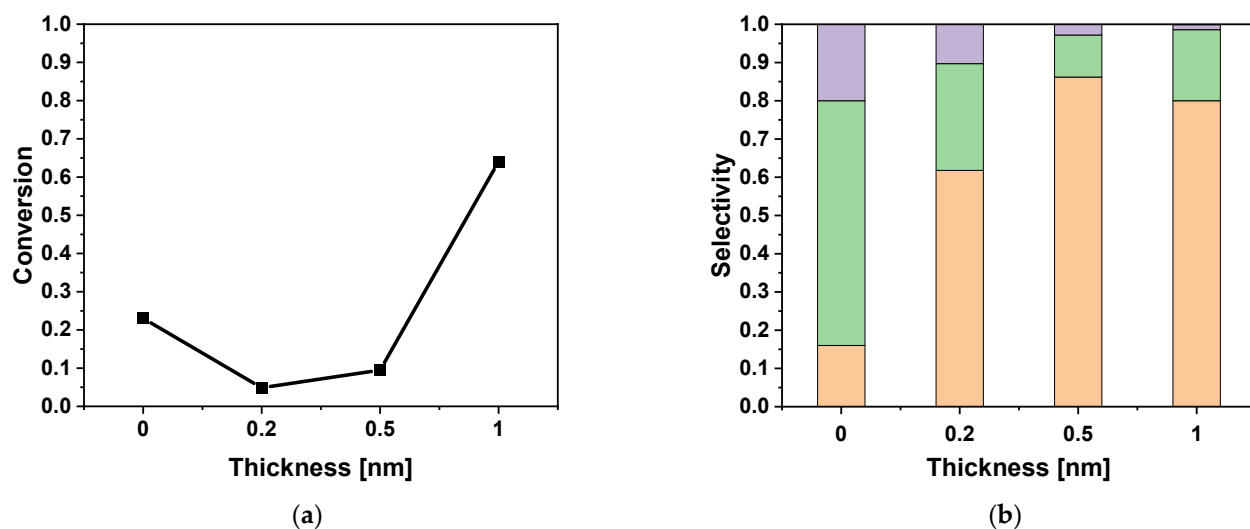

Figure 8. (**a**) THF conversion at 673 K on MAO and on 0.2 nm, 0.5 nm, and 1 nm ZrO$_2$ films on MAO (WHSV = 1.86 g THF/g cat/h). (**b**) The corresponding product selectivities: orange (bottom)-butadiene; green (middle)-propene; purple-butene (top).

To further investigate support effects, we also examined the reactivity of ALD-grown ZrO_2 films on silica films with a thickness of 0.2 nm (11 wt%), 0.5 nm (28 wt%), and 1 nm (56 wt%). Figure 9 shows conversion and selectivity for the reaction of THF on ZrO_2-SiO_2 ALD samples at 673 K as a function of the ZrO_2 film thickness. Data for a ZrO_2-SiO_2 sample where wet impregnation was used to deposit the ZrO_2 is also included for comparison. The ZrO_2 weight loading for the impregnated sample was 56 wt%, which corresponds approximately to the weight loading from a continuous 1 nm ZrO_2 film. It is worth noting that, for the conditions used, the bare SiO_2 support was relatively unreactive for THF dehydra-decyclization, with a conversion of less than 5%. The 0.2 nm ZrO_2-SiO_2 sample exhibited relatively low reactivity, with a THF conversion of only 4%, with limited selectivity to the desired dehydra-decyclization product butadiene (48%) and the rest being mostly propene. Increasing the ZrO_2 film thickness to 1 nm resulted in an increase in activity, with a THF conversion of 22%; however, the selectivity to butadiene remained low at only 41%. The impregnated ZrO_2-SiO_2 sample had a similar activity as the 1 nm ALD film, with a THF conversion of 22%; but the impregnated ZrO_2 sample exhibited a significantly higher selectivity to butadiene of 70%. For this impregnated sample, the ZrO_2 is likely in the form of small crystallites, rather than the continuous films present in the ALD samples. These results again highlight the fact that the reaction of THF on ZrO_2 is highly sensitive to the structure of the surface.
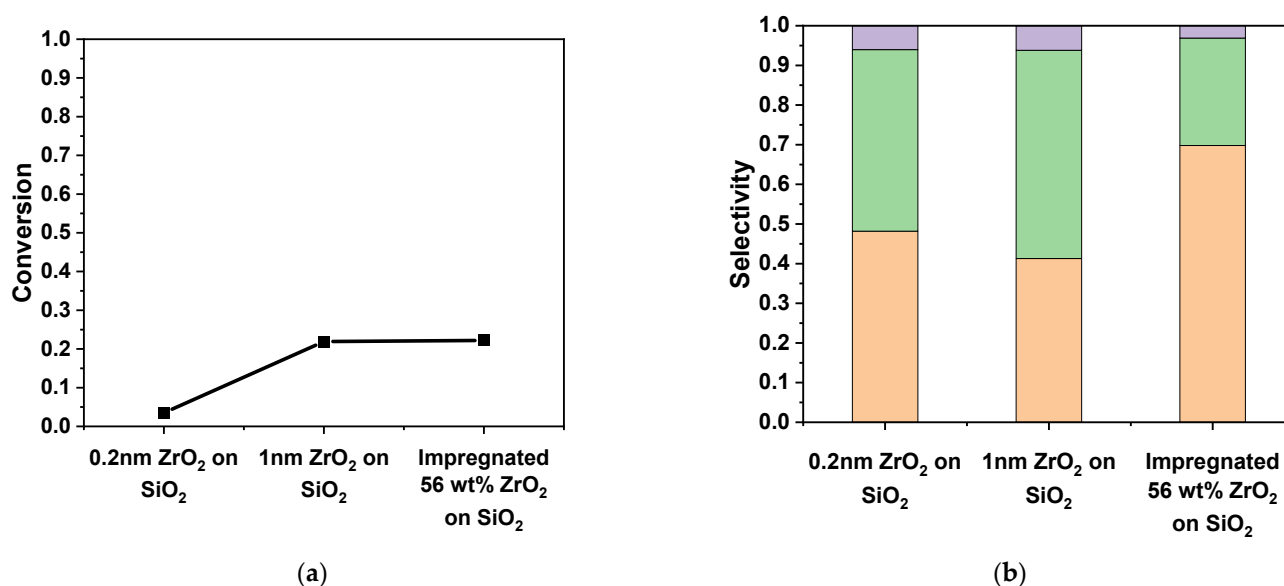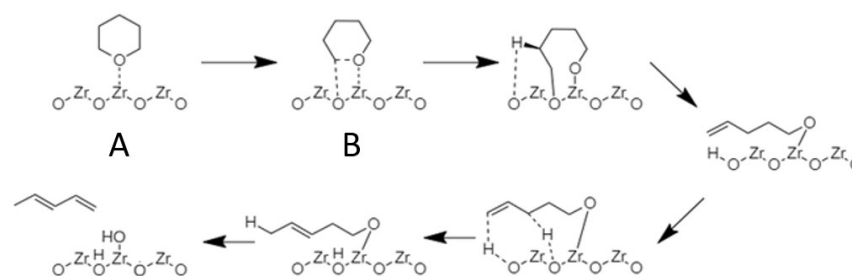

(a)   (b)

Figure 9. (**a**) THF conversion at 673 K on 0.2 nm, 1 nm, and impregnated 56 wt% ZrO_2-SiO_2 samples (WHSV = 1.86 g THF/g cat/h). (**b**) The corresponding product selectivities: orange-butadiene; green-propene; purple-butene.

3. Discussion

The data obtained for the Na-modified ZrO_2 surfaces revealed that adsorbed Na is highly effective at poisoning the activity for ring opening of the cyclic ethers, THF, and THP. To understand this result, it is useful to consider the recent work of Ji et al. [23] who used DFT calculations to predict the ring opening mechanism on zirconia. In that study, it was found that cyclic ethers adsorb on a tetragonal ZrO_2(101) surface via interaction of the lone pair electrons on the ring oxygen with a surface Lewis acidic Zr^{4+} site. The cleavage of the C-O bond to open the ring was predicted to proceed through a transition state in which the carbon is stabilized by interaction with an adjacent surface O^{2-} site, resulting in the formation of a 4-pentene-1-olate intermediate in which the oxygen remains coordinated to the Zr^{4+} and the C becomes coordinated to the O^{2-} site. A simplified version of this mechanism is shown in Scheme 2. By this mechanism, an adjacent surface Zr-O site pair is required for the ring opening to proceed. For Na-poisoned ZrO_2 samples, the most likely

binding sites for the adsorbed Na^+ ions are the surface lattice oxygens. This assumption is supported by FTIR data, which show that the Na did not block the Lewis acid sites on which pyridine adsorbed on ZrO_2 (see Figure S4). Thus, adsorbed Na does not block the Zr^{4+} site upon which cyclic ethers (or alcohols) initially adsorb (structure A in Scheme 2) but may be effective at blocking the Zr-O site pairs that are needed for ring opening as shown in structure B in Scheme 2. Thus, the results of the present study appear to be consistent with the Ji et al. DFT calculations for the ring opening mechanism. Since the surface lattice oxygens would also be involved in the dehydration of resulting adsorbed alkoxides to form the desired dienes, one would also expect adsorbed Na to affect this subsequent reaction. Although this is indeed the case, the decrease in the dehydration activity with Na coverage is less than that for the ring opening suggesting that hydrogen abstraction from the adsorbed alkoxides is less dependent on having an adjacent surface lattice oxygen. Although the reason for this is not clear, one possible explanation is that since the dehydration reaction (last step in Scheme 2) involves cleavage of a C-H bond in the β-position rather than the α-position, there are more surface oxygens that could participate in this reaction relative to the ring opening reaction, including both those that are the nearest neighbor and next-nearest neighbor to the Zr^{4+} alkoxide adsorption site.

Scheme 2. Proposed mechanism for dehydra-decyclization of THP on ZrO_2.

In addition to providing insight into the site requirements for the ring opening of cyclic ethers, the results obtained here also demonstrate that the reaction of these molecules on ZrO_2 is highly structure sensitive with different forms of ZrO_2 exhibiting different overall reactivities. Indeed, some forms of zirconia, such as the cubic Y-ZrO_2(110) and Y-ZrO_2(100) surfaces appear to be completely inactive for ring opening. The ideal cubic ZrO_2(100) surface is terminated by a layer of only four-fold coordinate Zr^{4+} cations, which would be expected to provide strong binding sites for the ring oxygen in cyclic ethers [26,28], and the Y-ZrO_2(100) TPD data do indeed show considerable adsorption of THF on this surface. The exposed O^{2-} anions on this surface, however, are fully coordinated and this may make them less effective at stabilizing the ring opening transition state. This may explain why THF just desorbs intact from this surface. On cubic ZrO_2(110), the exposed Zr^{4+} cations are six-fold coordinates, and it has been proposed that they have a lower affinity for oxygen than those on cubic ZrO_2(100) [28]. This is also consistent with the TPD data, which show little adsorption of THF at 300 K on this surface.

The structure sensitivity of the reaction of cyclic ethers on ZrO_2 is also apparent in the data obtained for the ALD-grown ZrO_2-thin films on the MAO and SiO_2 supports. Both the TPD and steady-state reaction data in Figures 7 and 8 show that 0.2 and 0.5 nm ZrO_2 films on MAO are much less reactive for ring opening and subsequent dehydration of THF than a 1 nm ZrO_2 film on this support. Since, as shown in Figure 6, both the 0.5 and 1 nm ZrO_2 films cover the majority of the MAO surface, it is not possible to attribute the large difference in the activity of these samples to a coverage effect or the number of exposed Zr sites. Note that, as shown in Figure S1, the 1 nm ZrO_2 film produces an XRD pattern characteristic of tetragonal ZrO_2, demonstrating that for this thickness, the bulk crystal structure is well developed. Apparently, the 0.2 and 0.5 nm films expose Zr sites that vary substantially from those in the thicker more bulk-like 1 nm film. Although the origin of this effect is not discernible from these data, it is possible that the thinner films contain more

isolated Zr sites, which are either less reactive toward THF or do not contain the Zr-O site pairs, that are needed for ring opening. It is also possible that for the ultrathin films, the interaction/bonding with the support changes the reactivity of the exposed Zr and O sites in such a way that it makes them less reactive for the ring opening of cyclic ethers.

4. Materials and Methods

4.1. Catalyst Synthesis

Bulk ZrO_2 powder was synthesized by dissolving 1 g of zirconium oxynitrate hydrate ($ZrO(NO_3)_2 \cdot xH_2O$, 99%, Sigma Aldrich, Burlington, MA, USA) in 10 mL deionized water, after which the solution was dried at 333 K for 12 h. The resulting precipitate was then calcined in static air at 673 K for 5 h to form tetragonal ZrO_2, as determined by XRD, that had a BET surface area of 76 $m^2 \cdot g^{-1}$. Thin films of ZrO_2 were synthesized on high-surface-area $MgAl_2O_4$ (MAO, PURALOX MG26/100, 97 $m^2 \cdot g^{-1}$, Sasol Germany, Hamburg, Germany) and SiO_2 (Q-30, 99 $m^2 \cdot g^{-1}$, FUJI SILYSIA CHEMICAL Ltd., Greenville, NC, USA) supports by atomic layer deposition (ALD) using a home-built, vacuum ALD apparatus that has been previously described in detail [29,30]. To facilitate sample handling for ALD, the MAO and SiO_2 substrates were pressed into self-supporting wafers. They were pretreated by calcining at 773 K in static to remove surface contaminants and then loaded into the ALD apparatus. For each ALD cycle, the samples were exposed to the vapor of the $Zr(TMHD)_4$ (99%, Strem Chemicals, Newburyport, MA, USA) precursor at 523 K for 10 min. They were then transferred to a furnace and calcined at 773 K in static air for 10 min to oxidize the adsorbed precursor and form ZrO_2. This procedure was repeated as many times as necessary to produce a film of the desired thickness. We have previously reported on the synthesis of ZrO_2 films using this ALD procedure and shown, using STEM and EDS, that they are conformal to the surface of the oxide support [31].

The film thicknesses were calculated from the surface area of the substrate and the mass of ZrO_2 deposited, assuming the film had the same density as that of bulk ZrO_2. For both 1 nm-ZrO_2/MAO and 1 nm-ZrO_2/SiO_2 samples, the ZrO_2 films were predominantly in the tetragonal phase, although a small amount of monoclinic ZrO_2 was also present in both samples, as determined by XRD (see Figures S1 and S2). Wet impregnation was used as an alternative method of depositing ZrO_2 on the MAO support. This was accomplished by adsorbing a predetermined amount of an aqueous solution of zirconium oxynitrate hydrate ($ZrO(NO_3)_2 \cdot xH_2O$, 99%, Sigma Aldrich) onto the support, followed by drying and then calcination at 773 K for 1 h in static air. The XRD pattern for this sample contained peaks characteristic of monoclinic ZrO_2. Based on the XRD line widths, the ZrO_2 crystallite size for this sample was estimated to be 5 nm.

Sodium-poisoned ZrO_2 samples were used in some experiments. These samples were prepared by first removing any surface contamination from the ZrO_2 by submersing 1 g of the powder in 500 mL of a 1 M aqueous NH_4NO_3 solution at 353 K and stirring for 6 h. The ZrO_2 powder was then washed in deionized water and dried at 353 K overnight. Sodium was then absorbed onto the surface of the pretreated ZrO_2 by incipient wetness of a $NaNO_3$ solution, which contained the desired amount of Na, followed by drying at 353 K overnight and calcination in static air at 673 K for 2 h.

4.2. Catalyst Characterization

Temperature-programmed desorption, thermal-gravimetric-analysis (TPD-TGA) measurements of bulk and thin-film ZrO_2 samples were performed using a custom-built, turbomolecular-pumped vacuum system that housed a CAHN 2000 microbalance and a quadrupole mass spectrometer (Stanford Research Systems, Sunnyvale, CA, USA). In a typical TPD-TGA experiment, 20 mg of sample were placed in the sample pan of the microbalance and heated to 823 K under vacuum to remove any adsorbed species. After cooling to room temperature, the sample was exposed to the vapor of the reactant molecule until the surface of the sample was saturated. The sample was evacuated for 1 h and

then heated at 10 K/min to 823 K while the desorbing species were monitored with the quadrupole mass spectrometer.

TPD experiments were performed using yttria-stabilized zirconia (YSZ) single crystals that exposed either a (100) or (110) surface (MTI Corporation, Richmond, CA, USA). These experiments were performed in an ultra-high vacuum (UHV) chamber that had a background pressure less than 10^{-9} Torr and were equipped with a quadrupole mass spectrometer (Stanford Research Systems) for TPD and an ion gun for sample cleaning. The single-crystal samples were attached to the sample manipulator on the UHV chamber using a tantalum foil holder and a K-type thermocouple was glued to their back surface using a high-temperature, zirconia-based adhesive (Aremco Ultra-Temp 516). Once in vacuum, the single crystals were cleaned by sputtering with a 2 kV Ar$^+$ ion beam for 20 min, followed by annealing in 10^{-6} Torr of O$_2$ at 700 K for 1 h. For a TPD experiment, the sample at 300 K was exposed to 20 Langmuirs (1 L = 10^{-6} Torr-sec) of the reactant molecule using a variable leak valve. It was then positioned in front of the mass spectrometer and heated at 3 K/s while monitoring the desorbing species.

X-ray diffraction (XRD) patterns for the various samples were collected using a Rigaku MiniFlex diffractometer equipped with a Cu Kα source (λ = 154.05 pm). BET surface areas were measured using a home-built adsorption apparatus using N$_2$ as the adsorbent at 77 K. Reaction rates were measured using a tubular flow reactor (0.25-in stainless steel tube) that was placed in a tube furnace. In a typical reaction rate experiment, 100 mg of catalyst was placed in the reactor and held in place using glass wool. Liquid reactants, tetrahydrofuran (THF, $\geq$99.9%, Sigma Aldrich), tetrahydropyran (THP, 98+%, Alfa Aesar, Ward Hill, MA, USA), 4-penten-1-ol (4P1OL, 99%, Sigma Aldrich), or isopropanol (99.5% min, Alfa Aesar) were introduced into a 20 sccm stream of He (UHP 99.999%, Airgas, Radnor, PA, USA) using a syringe pump (PHD 2000 Infusion, Harvard Apparatus, Holliston, MA, USA). To avoid condensation of reactants and products, all lines were heated to 423 K using heating tapes. Conversions and product distributions were measured over a period of less than 2 h. No deactivation of the catalyst was observed over this time span. Products were analyzed using a GC-Mass Spec (QP5000, Shimadzu, Kyoto, Japan) and equipped with a capillary column (HP-INNOWAX, Agilent Technologies, Santa Clara, CA, USA). Blank reaction experiments in which no catalyst was present showed no conversion for both the cyclic ether and alcohol reactants.

Fourier transform infrared (FTIR) spectroscopy of pyridine dosed ZrO$_2$ samples was used to characterize surface Lewis and Brønsted acid sites. These spectra were collected using a Bruker Tensor II spectrometer equipped with a DLaTGS detector and mid-IR source. Additional details for the FTIR experiments are given in the supplemental information.

5. Conclusions

The results obtained in this study provide insight into the active sites for the dehydra-decyclization of cyclic ethers to produce dienes on ZrO$_2$ surfaces. Steady-state reactivity and TPD data both demonstrated that adsorbed Na was more effective at poisoning the sites required for ring opening of cyclic ethers relative to those required for dehydration of the resulting adsorbed alkoxides. Based on this result and previous DFT simulations [23], we speculate that this may be due to the Na -oxygen anion sites adjacent to the Zr cation sites upon which the cyclic ethers adsorb. It is not clear, however, why such sites appear to be less critical for the alkoxide dehydration reaction. The dehydra-decyclization of cyclic ethers was also found to be structure sensitive with different forms of ZrO$_2$ exhibiting different reactivities. For example, bulk tetragonal-ZrO$_2$ was found to be highly reactive and selective for the production of the desired conjugated dienes; cubic ZrO$_2$ single crystal surfaces that exposed (100) and (110) surfaces were inactive. For ultra-thin ZrO$_2$ films, high dehydra-decyclization selectivity was observed for 1 nm thick films with well-developed crystalline structure, but low conversion and selectivity were obtained for 0.2 and 0.5 nm thick films.

References

1. Liu, Q.; Zhang, T.; Liao, Y.; Cai, C.; Tan, J.; Wang, T.; Qiu, S.; He, M.; Ma, L. Production of C5/C6 Sugar Alcohols by Hydrolytic Hydrogenation of Raw Lignocellulosic Biomass over Zr Based Solid Acids Combined with Ru/C. *ACS Sustain. Chem. Eng.* **2017**, *5*, 5940–5950. [CrossRef]

2. Scholz, D.; Aellig, C.; Mondelli, C.; Pérez-Ramírez, J. Continuous Transfer Hydrogenation of Sugars to Alditols with Bioderived Donors over Cu–Ni–Al Catalysts. *ChemCatChem* **2015**, *7*, 1551–1558. [CrossRef]

3. Zhang, S.; Maréchal, F.; Gassner, M.; Périn-Levasseur, Z.; Qi, W.; Ren, Z.; Yan, Y.; Favrat, D. Process Modeling and Integration of Fuel Ethanol Production from Lignocellulosic Biomass Based on Double Acid Hydrolysis. *Energy Fuels* **2009**, *23*, 1759–1765. [CrossRef]

4. Haworth, W.N.; Jones, W.G.M. 183. The conversion of sucrose into furan compounds. Part I. 5-Hydroxymethylfurfuraldehyde and some derivatives. *J. Chem. Soc.* **1944**, 667–670. [CrossRef]

5. Tong, X.; Ma, Y.; Li, Y. Biomass into chemicals: Conversion of sugars to furan derivatives by catalytic processes. *Appl. Catal. A Gen.* **2010**, *385*, 1–13. [CrossRef]

6. Eerhart, A.J.J.E.; Huijgen, W.J.J.; Grisel, R.J.H.; van der Waal, J.C.; de Jong, E.; de Sousa Dias, A.; Faaij, A.P.C.; Patel, M.K. Fuels and plastics from lignocellulosic biomass via the furan pathway; a technical analysis. *RSC Adv.* **2014**, *4*, 3536–3549. [CrossRef]

7. Chernyshev, V.M.; Kravchenko, O.A.; Ananikov, V.P. Conversion of plant biomass to furan derivatives and sustainable access to the new generation of polymers, functional materials and fuels. *Russ. Chem. Rev.* **2017**, *86*, 357–387. [CrossRef]

8. Liu, S.; Josephson, T.R.; Athaley, A.; Chen, Q.P.; Norton, A.; Ierapetritou, M.; Siepmann, J.I.; Saha, B.; Vlachos, D.G. Renewable lubricants with tailored molecular architecture. *Sci. Adv.* **2019**, *5*, eaav5487. [CrossRef]

9. Norton, A.M.; Liu, S.; Saha, B.; Vlachos, D.G. Branched Bio-Lubricant Base Oil Production through Aldol Condensation. *ChemSusChem* **2019**, *12*, 4780–4785. [CrossRef]

10. Abdelrahman, O.A.; Park, D.S.; Vinter, K.P.; Spanjers, C.S.; Ren, L.; Cho, H.J.; Vlachos, D.G.; Fan, W.; Tsapatsis, M.; Dauenhauer, P.J. Biomass-Derived Butadiene by Dehydra-Decyclization of Tetrahydrofuran. *ACS Sustain. Chem. Eng.* **2017**, *5*, 3732–3736. [CrossRef]

11. Makshina, E.V.; Dusselier, M.; Janssens, W.; Degrève, J.; Jacobs, P.A.; Sels, B.F. Review of old chemistry and new catalytic advances in the on-purpose synthesis of butadiene. *Chem. Soc. Rev.* **2014**, *43*, 7917–7953. [CrossRef]

12. Abdelrahman, O.A.; Park, D.S.; Vinter, K.P.; Spanjers, C.S.; Ren, L.; Cho, H.J.; Zhang, K.; Fan, W.; Tsapatsis, M.; Dauenhauer, P.J. Renewable Isoprene by Sequential Hydrogenation of Itaconic Acid and Dehydra-Decyclization of 3-Methyl-Tetrahydrofuran. *ACS Catal.* **2017**, *7*, 1428–1431. [CrossRef]

13. Olivera, S.; Muralidhara, H.B.; Venkatesh, K.; Gopalakrishna, K.; Vivek, C.S. Plating on acrylonitrile–butadiene–styrene (ABS) plastic: A review. *J. Mater. Sci.* **2016**, *51*, 3657–3674. [CrossRef]

14. Blanco, D.E.; Dookhith, A.Z.; Modestino, M.A. Enhancing selectivity and efficiency in the electrochemical synthesis of adiponitrile. *React. Chem. Eng.* **2019**, *4*, 8–16. [CrossRef]

15. Kumbhalkar, M.D.; Buchanan, J.S.; Huber, G.W.; Dumesic, J.A. Ring Opening of Biomass-Derived Cyclic Ethers to Dienes over Silica/Alumina. *ACS Catal.* **2017**, *7*, 5248–5256. [CrossRef]

16. Li, S.; Abdelrahman, O.A.; Kumar, G.; Tsapatsis, M.; Vlachos, D.G.; Caratzoulas, S.; Dauenhauer, P.J. Dehydra-Decyclization of Tetrahydrofuran on H-ZSM5: Mechanisms, Pathways, and Transition State Entropy. *ACS Catal.* **2019**, *9*, 10279–10293. [CrossRef]

17. Yu, J.; Zhu, S.; Dauenhauer, P.J.; Cho, H.J.; Fan, W.; Gorte, R.J. Adsorption and reaction properties of SnBEA, ZrBEA and H-BEA for the formation of p-xylene from DMF and ethylene. *Catal. Sci. Technol.* **2016**, *6*, 5729–5736. [CrossRef]

18. Xu, M.; Mukarakate, C.; Iisa, K.; Budhi, S.; Menart, M.; Davidson, M.; Robichaud, D.J.; Nimlos, M.R.; Trewyn, B.G.; Richards, R.M. Deactivation of Multilayered MFI Nanosheet Zeolite during Upgrading of Biomass Pyrolysis Vapors. *ACS Sustain. Chem. Eng.* **2017**, *5*, 5477–5484. [CrossRef]
19. Kumar, G.; Liu, D.; Xu, D.; Ren, L.; Tsapatsis, M.; Dauenhauer, P.J. Dehydra-decyclization of 2-methyltetrahydrofuran to pentadienes on boron-containing zeolites. *Green Chem.* **2020**, *22*, 4147–4160. [CrossRef]
20. Ji, Y.; Lawal, A.; Nyholm, A.; Gorte, R.J.; Abdelrahman, O.A. Dehydra-decyclization of tetrahydrofurans to diene monomers over metal oxides. *Catal. Sci. Technol.* **2020**, *10*, 5903–5912. [CrossRef]
21. Kozlowski, J.T.; Davis, R.J. Sodium modification of zirconia catalysts for ethanol coupling to 1-butanol. *J. Energy Chem.* **2013**, *22*, 58–64. [CrossRef]
22. Wang, C.; Mao, X.; Lee, J.; Onn, T.; Yeh, Y.-H.; Murray, C.; Gorte, R. A Characterization Study of Reactive Sites in ALD-Synthesized WOx/ZrO2 Catalysts. *Catalysts* **2018**, *8*, 292. [CrossRef]
23. Ji, Y.; Batchu, S.P.; Lawal, A.; Vlachos, D.G.; Gorte, R.J.; Caratzoulas, S.; Abdelrahman, O.A. Selective dehydra-decyclization of cyclic ethers to conjugated dienes over zirconia. *J. Catal.* **2022**, *410*, 10–21. [CrossRef]
24. Sayan, S.; Nguyen, N.V.; Ehrstein, J.; Emge, T.; Garfunkel, E.; Croft, M.; Zhao, X.; Vanderbilt, D.; Levin, I.; Gusev, E.P.; et al. Structural, electronic, and dielectric properties of ultrathin zirconia films on silicon. *Appl. Phys. Lett.* **2005**, *86*, 152902. [CrossRef]
25. Martono, E.; Vohs, J.M. Active Sites for the Reaction of Ethanol to Acetaldehyde on Co/YSZ(100) Model Steam Reforming Catalysts. *ACS Catal.* **2011**, *1*, 1414–1420. [CrossRef]
26. Dilara, P.A.; Vohs, J.M. Structure sensitivity in the reaction of methanol on ZrO_2. *Surf. Sci.* **1994**, *321*, 8–18. [CrossRef]
27. Gao, M.; Zhang, M.; Yu, Y. Study on the Reaction Species of 1, 3-Butadiene Formation from Bio-ethanol on ZrO_2. *Catal. Lett.* **2016**, *146*, 2450–2457. [CrossRef]
28. Han, Y.; Zhu, J. Surface Science Studies on the Zirconia-Based Model Catalysts. *Top. Catal.* **2013**, *56*, 1525–1541. [CrossRef]
29. Onn, T.M.; Arroyo-Ramirez, L.; Monai, M.; Oh, T.-S.; Talati, M.; Fornasiero, P.; Gorte, R.J.; Khader, M.M. Modification of Pd/CeO2 catalyst by Atomic Layer Deposition of ZrO_2. *Appl. Catal. B Environ.* **2016**, *197*, 280–285. [CrossRef]
30. Onn, T.M.; Zhang, S.; Arroyo-Ramirez, L.; Xia, Y.; Wang, C.; Pan, X.; Graham, G.W.; Gorte, R.J. High-surface-area ceria prepared by ALD on Al_2O_3 support. *Appl. Catal. B Environ.* **2017**, *201*, 430–437. [CrossRef]
31. Onn, T.M.; Zhang, S.; Arroyo-Ramirez, L.; Chung, Y.-C.; Graham, G.W.; Pan, X.; Gorte, R.J. Improved Thermal Stability and Methane-Oxidation Activity of Pd/Al_2O_3 Catalysts by Atomic Layer Deposition of ZrO_2. *ACS Catal.* **2015**, *5*, 5696–5701. [CrossRef]